

# Numerical Simulation of the Turbulent Flow Around a Wing

Torsten Auerswald <sup>\*</sup> and Jens Bange <sup>†</sup>

*Center for Applied Geoscience, Universität Tübingen, Germany*

## Abstract

**The goal of the work presented in this paper is to simulate the influence of turbulent flow around a wing in the atmospheric boundary layer. For this purpose a method to generate synthetic turbulence with realistic characteristics is presented and compared to data from an LES of the atmospheric boundary layer. Furthermore, first simulation results without a wing are presented.**

## 1 Introduction

The influence of atmospheric turbulence on an aircraft is an important issue in many aspects of aviation. Since two of the most critical maneuvers, take-off and landing, are taking place in the atmospheric boundary layer (ABL), knowledge about the influence of atmospheric turbulent flow on aircraft aerodynamics is important for the safety and design of aircraft.

This paper presents a strategy to simulate the turbulent flow around a wing realistically. Today's computers are not powerful enough to simulate the flight of an aircraft through a complete ABL. Therefore, some simplifications have to be applied. First of all, not the complete aircraft is simulated but only the wing. And secondly, only a small section of the ABL is simulated by using synthetic turbulence which possesses important characteristics of real ABL turbulence. To generate this synthetic turbulence, high-resolution measurements from the ABL are used. Their statistics are calculated and used by a turbulence generator to generate a 3D synthetic turbulent wind field with the same statistical characteristics as the measurement data. These input statistics for the turbulence generator are the energy spectrum, the variances and the correlations of the wind-vector components. The generated wind field serves as initial wind field for a CFD model with which the flow around the wing is simulated.

As basis for the generation of the turbulent wind field the Fourier approach is used, in which the sum is taken over several waves with different wavenumbers to build a random velocity field. Comparable approaches were applied in earlier works by i.e. Kraichnan (1970) or Fung and Vassilicos (1998). The resulting velocity field is isotropic, Gaussian and reproduces a given energy spectrum. It can be modified by applying the Cholesky method to obtain a predefined anisotropic correlation matrix.

---

<sup>\*</sup>Project Scientist

<sup>†</sup>Project Leader

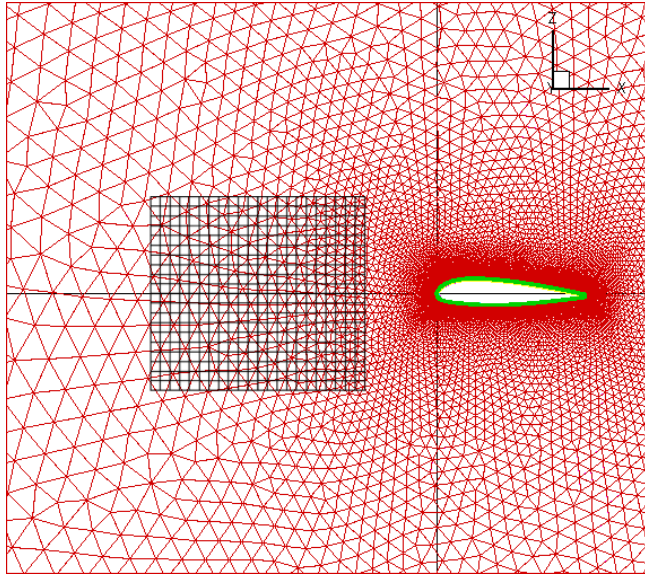


Figure 1: *Sketch of the model domain for the Chimera simulations with TAU. The domain consists of two grids. The primary grid (red) is body-fitted around the airfoil. The secondary Cartesian grid (red) is used to simulate the turbulent flow in front of the airfoil.*

## 2 Method

### 2.1 Modelling strategy

For the simulation of the turbulent flow around the airfoil the compressible flow solver TAU is used. TAU is developed by the German Aerospace Center (DLR) and allows for the usage of Chimera grids. In Fig. 1 a sketch of the model domain is presented. It consists of a Cartesian grid in front of the wing where the turbulent flow is initialised, and an unstructured grid which is body-fitted around the wing. During the model run the Cartesian grid is moved towards the wing. In a certain distance in front of the wing the Cartesian grid is stopped and the turbulent flow is passed to the body-fitted grid where it can interact with the wing.

To illustrate this strategy, results from a 2D test case are shown in Fig. 2. The test case is based on the work of Wolf *et al.* (2010) and shows the aforementioned sequence for a 2D simulation using Chimera in TAU where the flow field in the Cartesian grid was initialised with an analytical vortex. To investigate how the synthetic turbulence develops during a model run in TAU a test run was designed on a cubic Cartesian grid with  $500^3$  grid points and a grid spacing of 0.7 m. The time step in these simulations is  $10^{-3}$  s. In later simulation the same Cartesian grid will be used within the Chimera grid to simulate the flow around the wing.

### 2.2 The Turbulence Generator

Since the modelling domain does not contain the earth surface, there is no mechanism for developing ABL turbulence within the flow model. Therefore, the simulations have to be initialised with a turbulent wind field. For the wind field to be realistic, data measured by the Helipod (Bange *et al.*, 2007) is used. The Helipod is an airborne measurement probe which is attached to a helicopter. It was operated on several campaigns taking measurements in the ABL over land surface and the Arctic sea. Measurements were taken at altitudes between 40 m and 2000 m. Several sensors (e.g. wind vector, temperature, humidity) sampled at

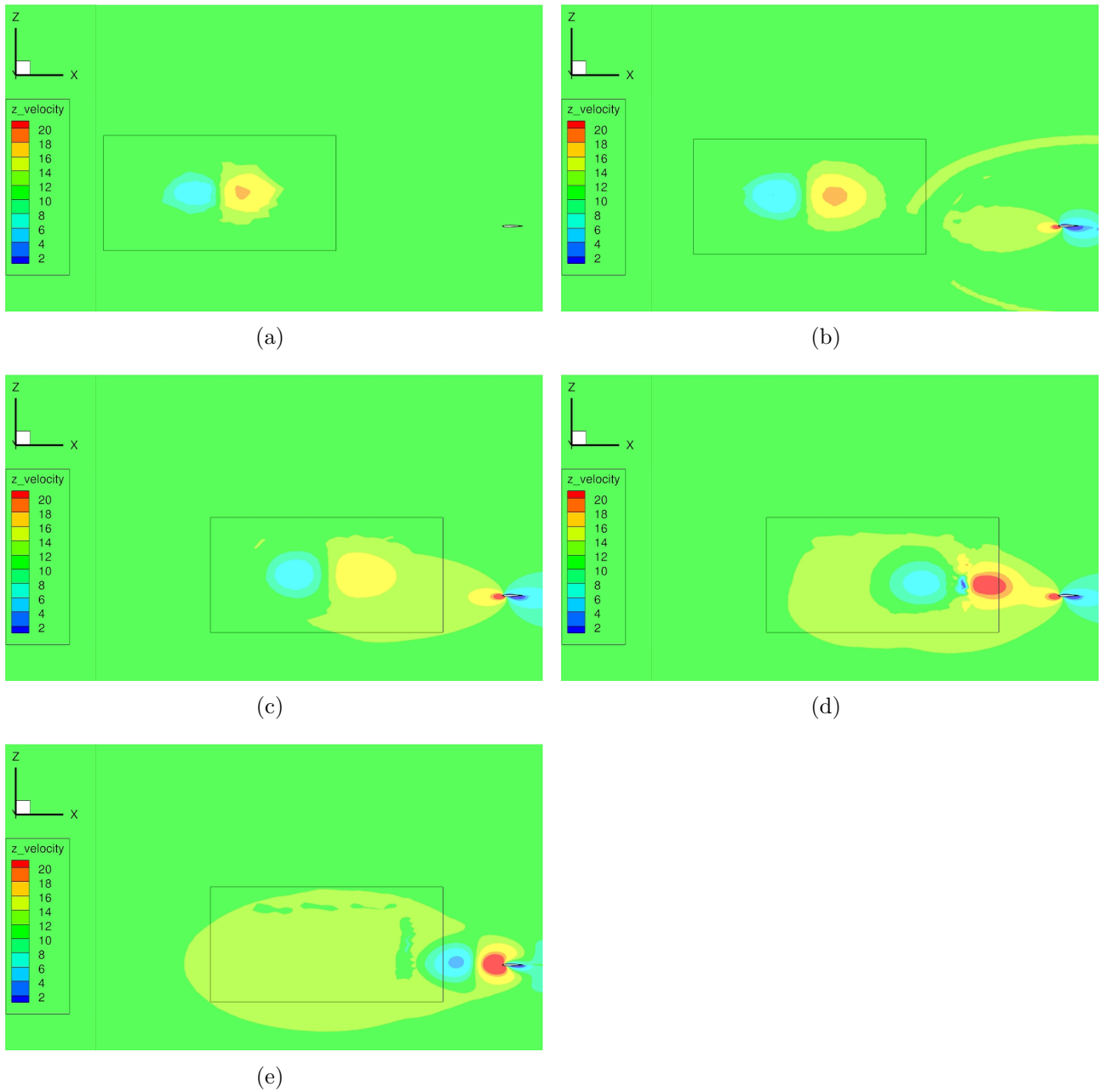


Figure 2: Results for the vertical velocity (in m/s) from the 2D test case using the Chimera method in TAU. The black box represents the Cartesian grid. The simulation is initialised with an analytical vortex.

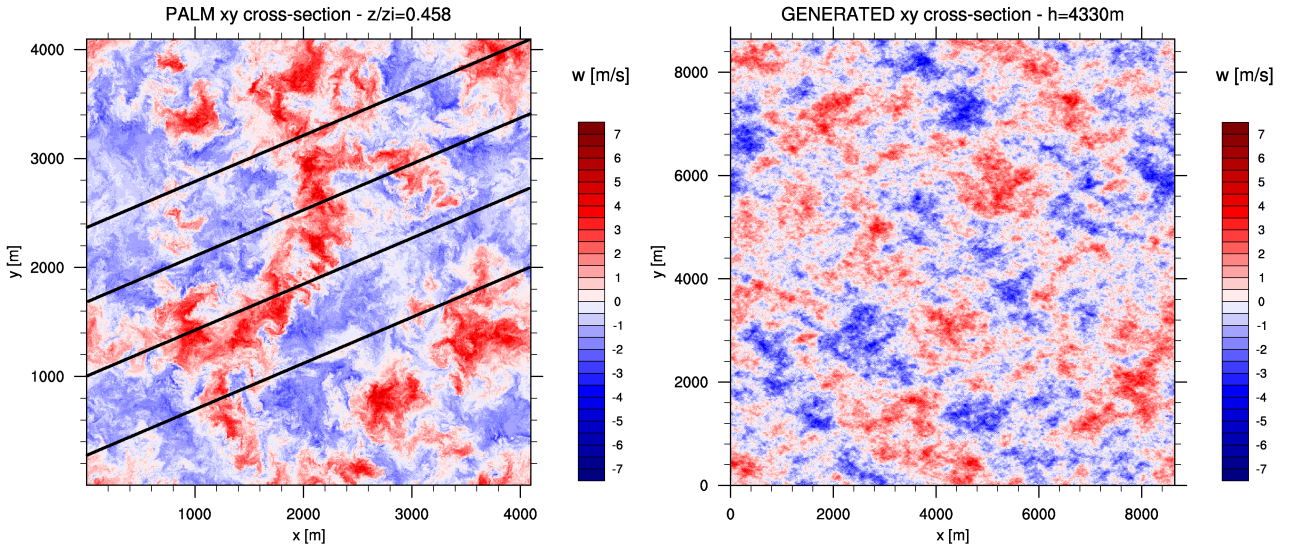


Figure 3: Comparison of vertical velocities in a horizontal cut plane through the PALM domain (left) and the synthetic turbulent wind field (right). The black lines in the PALM domain are indicating the flight pattern for the virtual measurement flights.

100 Hz (corresponding to about 40 cm distance between individual measurements) are mounted for high-resolution measurements in the ABL. A large data set of measurements for different meteorological scenarios is available including atmospheric flow in various thermal stratifications (stable, very stable, neutral, convective).

The turbulence generator that is used to generate the synthetic turbulence is based on the Fourier approach (for more details see Auerswald *et al.*, 2012):

$$\vec{v}(\vec{x}) = \sum_{n=1}^N \sum_{m=1}^N \sum_{l=1}^N \left( \vec{C}_{n,m,l} (\cos(\vec{k}_{n,m,l} \cdot \vec{x}) + i \sin(\vec{k}_{n,m,l} \cdot \vec{x})) \right),$$

where  $\vec{C}$  is the amplitude vector,  $\vec{k}$  is the wavenumber vector and  $\vec{x}$  is the position vector. By calculating the absolute value of the amplitude vector using:

$$|\vec{C}_{n,m,l}| = \sqrt{E(|\vec{k}_{n,m,l}|) \Delta |\vec{k}_{n,m,l}|},$$

the measured energy spectrum  $E(k)$  can be reproduced in the synthetic turbulence. The resulting wind field is divergence-free and isotropic. By applying the Cholesky decomposition (e.g. Lund *et al.*, 1998), the wind field can be modified to possess a predefined correlation matrix which introduces anisotropy in the turbulent flow. With a simple scaling of the resulting wind field the variances from the measurement can be introduced.

## 3 Results

A more detailed and extensive overview over the results can be found in Auerswald *et al.* (2012).

### 3.1 Turbulence Generator

Since 3D-measurement data from the ABL are not available, LES data of the ABL are used as a reference for the synthetic turbulence (see Auerswald *et al.*, 2010, for more details of the

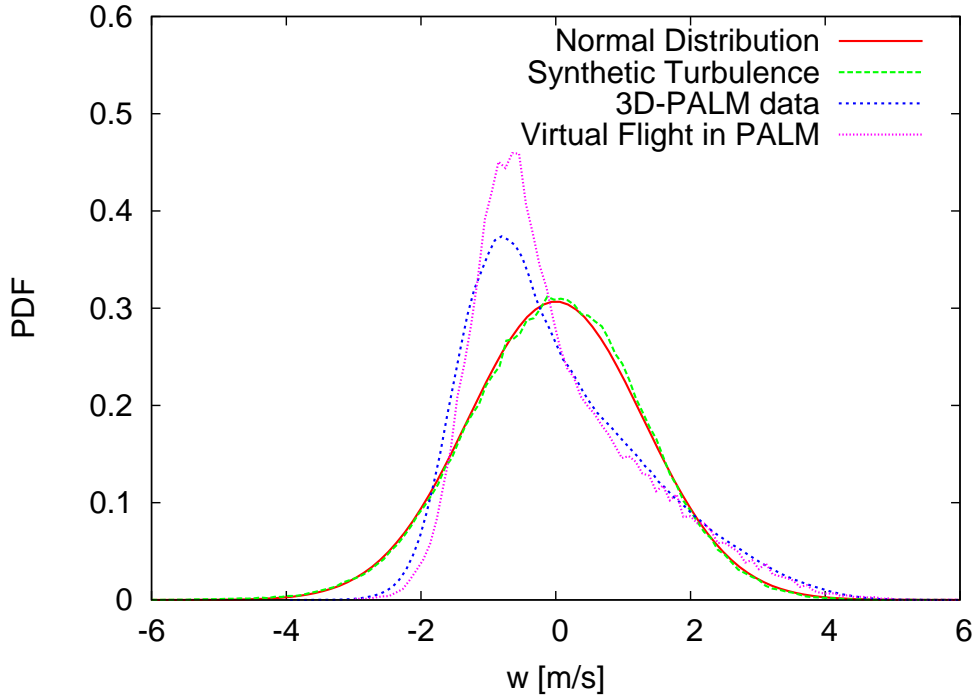


Figure 4: *PDF of the vertical velocity from the whole PALM domain (blue), the virtual measurements (pink) and the synthetic turbulence (green). As reference the normal distribution with the variance of the synthetic turbulence is plotted (red).*

comparison). The LES was carried out using the parallelized LES Model (PALM). To gather data comparable to the Helipod flights, virtual measurements flights were performed within the model domain. The statistics of the resulting time series were used to generate a synthetic turbulent wind field. A comparison of the vertical velocity in a horizontal cut plane through the PALM domain and the synthetic turbulence is given in Fig. 3. It is obvious that the structure of the turbulence in both fields is quite different. There are coherent structures in the PALM simulation comparable to the structures found in a real ABL. They appear as organised patterns of up and down drafts while in the synthetic wind field up and down drafts are randomly and equally distributed.

The same characteristics can be found in the probability density function (PDF) of the vertical velocity (see Fig. 4). The PDF of the vertical velocity of the whole model domain (blue) as well as the one of the virtual aircraft measurements (pink) are skewed while the PDF of the synthetic turbulence (green) is normally distributed (red). In the PALM domain there are many weak down drafts and few but strong updrafts, which is in line with the theory and measurements of the ABL. In contrast to that the updrafts and downdrafts are equally distributed in the synthetic wind field.

In the following, the statistics that were used as input for the turbulence generator are compared to the statistics of the resulting synthetic turbulence field. For this comparison data measured by the Helipod were used. In Fig. 5 the energy spectra from the Helipod measurement and from the synthetic turbulent wind field are shown. The spectra match very well (note that the spectrum from the generated field is shifted for better comparison). Both spectra follow the  $k^{-5/3}$ -slope of the inertial subrange. Since the Helipod measurement covers a much larger distance than the domain in which the synthetic turbulence was generated in, the spectrum from the measurement resolves much larger scales.

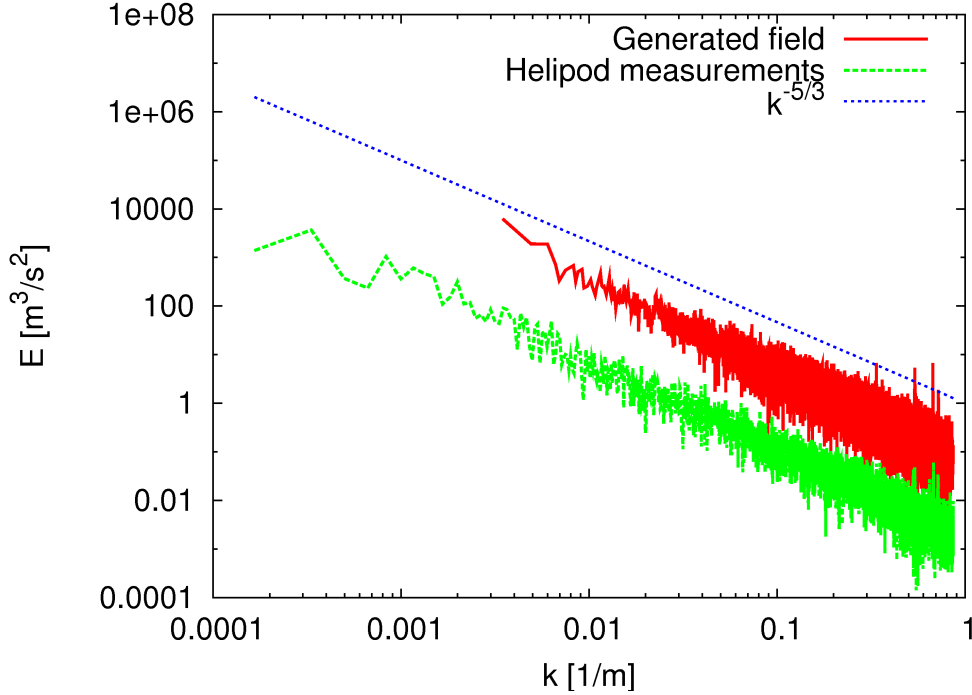


Figure 5: *Energy spectrum from the synthetic wind field (red) and the Helipod measurements (green). Note that the spectrum from the synthetic wind field was shifted to higher energies for better visibility. As a reference the  $k^{-5/3}$ -slope is plotted in blue.*

<u>Helipod measurements</u>				<u>Generated field</u>			
	$u'$	$v'$	$w'$		$u'$	$v'$	$w'$
$u'$	1	0.087	0.119	$u'$	1	0.079	0.097
$v'$	0.087	1	-0.004	$v'$	0.079	1	-0.005
$w'$	0.119	-0.004	1	$w'$	0.097	-0.005	1

Table 1: *Correlation matrices calculated from the Helipod measurements (left) and the synthetic wind field (right).*

In Tab. 1 the one-point correlations for the components of the wind vector are printed. There are only small deviations in the correlations of the synthetic wind field from the measurements. The anisotropy in the one point correlations of the measurements are represented very well in the synthetic turbulence.

### 3.2 TAU Simulation

In a first TAU simulation the synthetic turbulent wind field, produced from the Helipod data, was used to initialise the TAU model. In this run only the Cartesian grid (see Fig. 1) was used to see how the synthetic turbulence behaves in the model and how the statistics develop during the simulation. The Cartesian grid consists of  $500^3$  grid points and has a grid spacing of 0.7 m.

Fig. 6 shows the energy spectrum of the initial wind field and of the wind field after 3 s simulation time. It can be seen that after 3 s most of the energy spectrum still follows the  $k^{-5/3}$ -slope. The energy spectrum is shifted towards lower energies. Since there is no source for turbulent

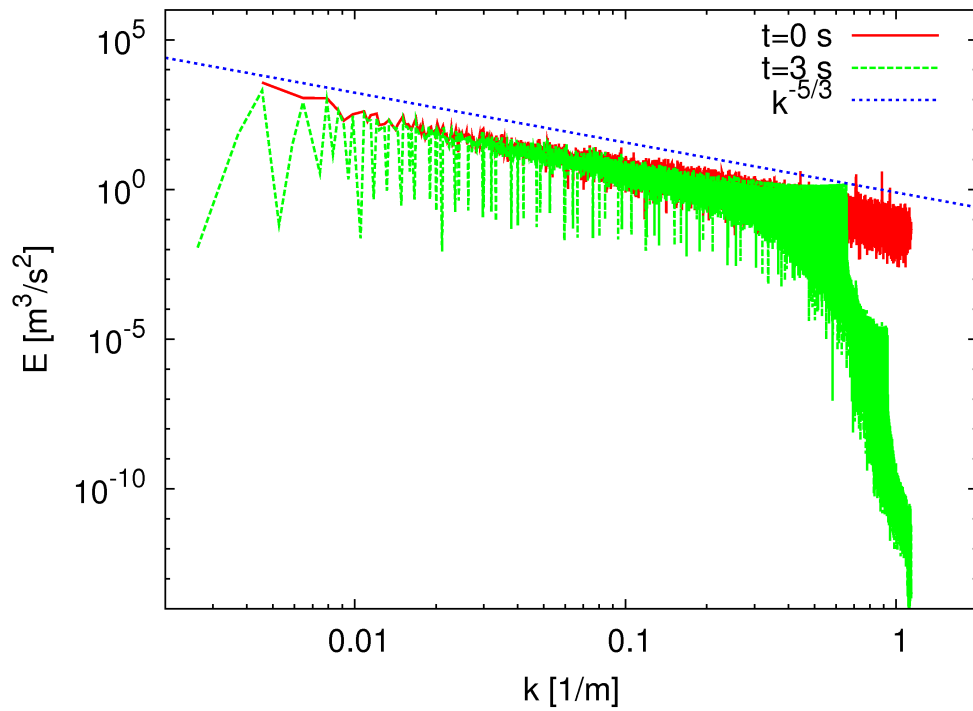


Figure 6: Energy spectrum from the initial wind field (red) and the wind field after 3 s simulation time (green). As a reference the  $k^{-5/3}$ -slope is plotted in blue.

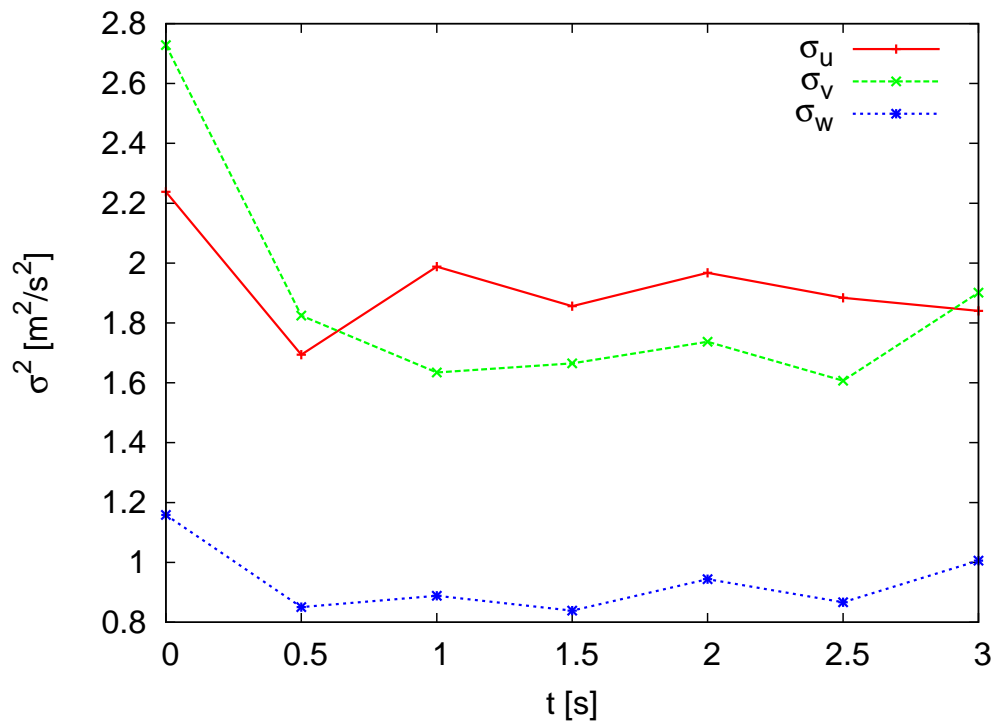


Figure 7: Timely development of the variance of the components of the velocity vector ( $\sigma_u$  - red,  $\sigma_v$  - green and  $\sigma_w$  - blue).

kinetic energy (TKE) in the model domain, the energy is decaying with time. Also noticeable is a significant loss of energy in the small scales, which is due to numerical dissipation and is typical behaviour of LES models. The loss of energy starts at wavenumbers that correspond to wavelengths of around four times the grid spacing. Wave numbers lower than this are unaffected. The significant troughs in the spectrum after 3 s are caused by wavenumber vectors for which one or more components equal zero. The energy of those wavenumbers was set to zero in the initial wind field resulting in zero mean velocity in the respective direction. During the simulation, energy from neighboring wavenumbers is transferred to these wavenumbers leading to the troughs in the spectrum.

The decay of TKE can also be seen in the development of the variances of the wind components (see Fig. 7). It exhibits a strong loss of energy towards the beginning of the simulation. After 0.5 s the variances stay on a more or less constant level.

The development of the one-point correlation coefficients is shown in Fig. 8. While in theory a return to isotropy is expected, the behaviour in the TAU model looks somewhat chaotic. It has to be stated though, that the simulation time is too short to make a qualitative statement about the development towards isotropy, which is expected to act on much larger time scales. An important feature of real atmospheric flows is intermittency which can be detected in the PDFs of the velocity increments. Fig. 9 shows the PDFs of the velocity increments of the velocity component in x-direction after 3 s simulation time for different separation distances  $s$ . While initially the PDFs of the increments were normally distributed for all separation distances, they develop tails at the ends of the distribution indicating the presence of intermittent events in the flow. The deviation from the normal distribution is stronger for smaller distances. For larger separation distances the PDFs become almost Gaussian. This behaviour is in line with the theory and measurement results from the ABL (Sreenivasan and Antonia, 1997).

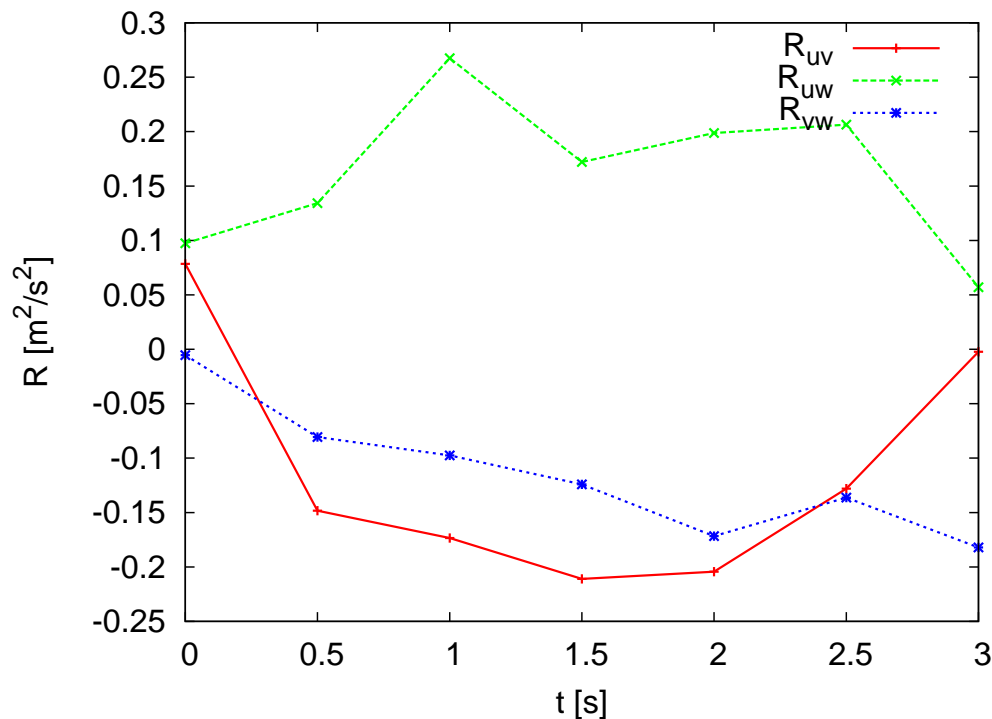


Figure 8: *Timely development of the one point correlation of u and v (red), u and w (green) and v and w (blue).*



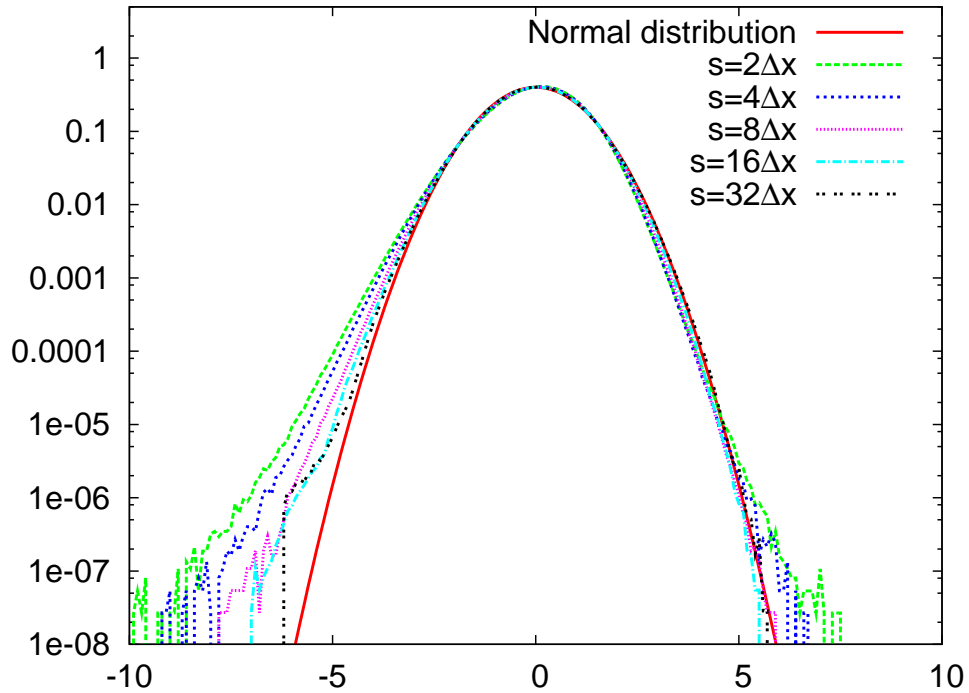


Figure 9: *PDFs of the velocity increments of  $u$  for separation distances  $s = 2\Delta x$  (green),  $s = 4\Delta x$  (blue),  $s = 8\Delta x$  (pink),  $s = 16\Delta x$  (light blue) and  $s = 32\Delta x$  (black). For comparison the normal distribution is plotted in red.*

## 4 Conclusion

The goal of the presented project is to investigate the influence of atmospheric turbulence on an aircraft wing using the flow model TAU. For this purpose a synthetic turbulence generator was defined which was used to initialise the flow model. The generated turbulent wind field showed some of the important features of real atmospheric turbulence. Especially, the input statistics were represented very well in the generated field. A comparison with an LES of the ABL showed some differences in the characteristics of the turbulence. The lack of coherent structures and therefore the difference in the distribution of the updrafts and downdrafts was one of the most significant differences.

Nevertheless, the turbulence generator was used to initialise the flow model in a first test run using only a Cartesian grid without a wing. The development of the spectral energy showed that the general shape was not changed for parts of the spectrum. Only a relatively small part at the high wavenumbers was lost due to numerical dissipation. Furthermore, the energy was preserved quite well during the model run. The development of the variances showed a quick drop in energy only in the first 0.5 s. For the rest of the simulation the variances remained at a more or less constant level.

Not much interpretation was possible for the timely development of the one point correlation coefficients. The expected return to isotropy could not be found. But since the simulation time was very short a qualitative statement can not be made.

Since it was shown that the turbulence generator delivers decent turbulent wind fields possessing important features of the real ABL and the TAU model can be initialised with this wind field,

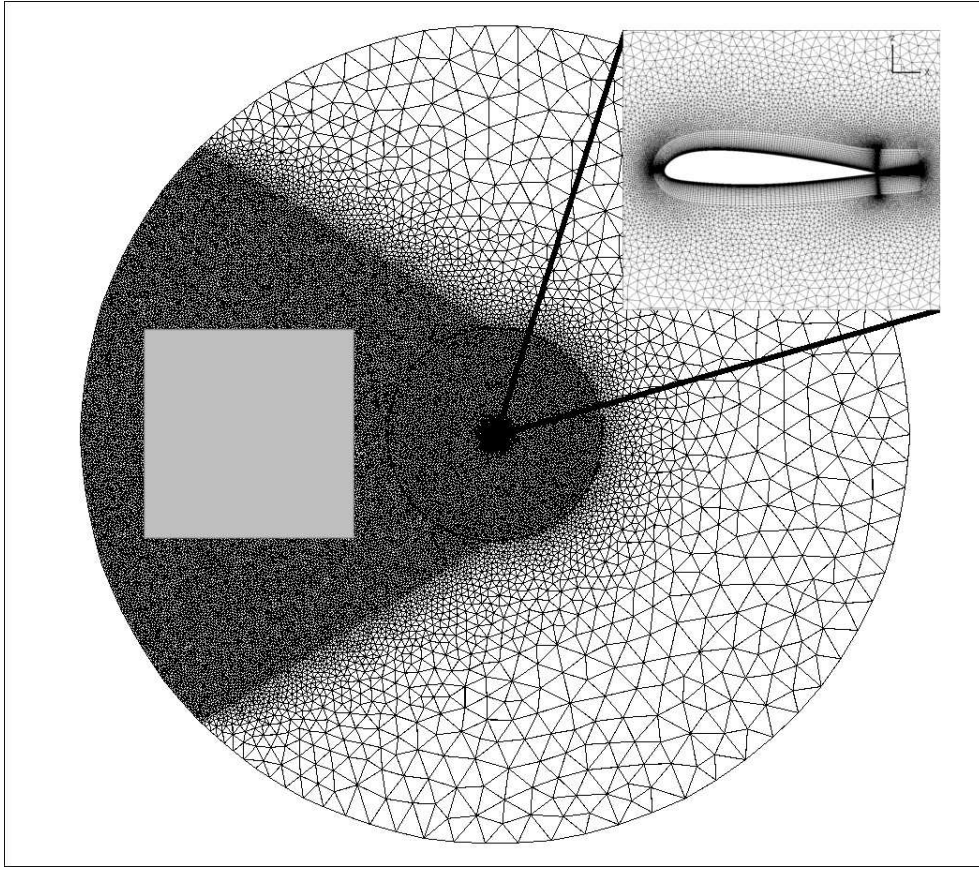


Figure 10: *Chimera grid for the TAU simulation of the flow around the wing. The grey block is representing the Cartesian grid.*

simulations are planned using the full chimera grid. The grid that will be used for these final simulations is depicted in Fig. 10. The grey block in front of the wing represents the Cartesian grid with a resolution of 0.7 m. The resolution of the body-fitted grid around the wing ranges from  $5 \cdot 10^{-6}$  m near the wing to 40 m in the outer region of the model domain. In front of the wing the resolution was increased to allow for better interpolation of the chimera algorithm between the Cartesian and the body-fitted grid. The total number of points for this grid is about 130 million. Results from these simulations will be presented in future publications.

## Acknowledgments

The members of the FOR 1066 research group gratefully acknowledge the support of the "Deutsche Forschungsgemeinschaft DFG" (German Research Foundation) which funded this research. We also thank the "North-German Supercomputing Alliance" (HLRN) for providing the resources to perform the simulations presented in this paper.

## References

**Auerswald, T., Weinreis, C., Bange, J., Raasch, S. and Radespiel, R., 2010:** Comparison Of High Resolution Large-Eddy Simulations And Synthetic Turbulent Wind Fields.

*AIAA Paper 2010-1253, 48th AIAA Aerospace Sciences Meeting Including the New Horizons Forum and Aerospace Exposition.*

- Auerswald, T., Bange, J., Knopp, T., Weinman, K. and Radespiel, R., 2012:** Large-Eddy Simulations of realistic atmospheric turbulence with the DLR-TAU-code initialized by in situ airborne measurements. *Computers & Fluids*, **66**, 121–129.
- Bange, J., Spieß, T. and van den Kroonenberg, A., 2007:** Characteristics of the Early-Morning Shallow Convective Boundary Layer from Helipod Flights during STINHO-2. *Theor. Appl. Climatol.*, **90**, 113–126.
- Fung, J. C. H. and Vassilicos, J. C., 1998:** Two-particle dispersion in turbulent like flows. *Physical Reviews E*, **57**, 1677–1690.
- Kraichnan, R. H., 1970:** Diffusion by a Random Velocity Field. *The Physics of Fluids*, **13**, 22–31.
- Lund, T. S., Wu, X. and Squires, K. D., 1998:** Generation of Turbulent Inflow Data for Spatially-Developing Boundary Layer Simulations. *J. Comput. Phys.*, **140**, 233–258.
- Sreenivasan, K. R. and Antonia, R. A., 1997:** The phenomenology of small-scale turbulence. *Annu. Rev. Fluid Mech.*, **29**, 435–472.
- Wolf, C., Raichle, A., Knopp, T. and Schwamborn, D., 2010:** Chimera Simulations of Transported Large-Scale Vortices and Their Interaction with Airfoils. In: *New Results in Numerical and Experimental Fluid Mechanics VII*, Springer Berlin / Heidelberg, *Notes on Numerical Fluid Mechanics and Multidisciplinary Design*, vol. 112, pp. 117–124.